INTERNATIONAL JOURNAL OF AUTOMOTIVE SCIENCE AND TECHNOLOGY

2026, VOL. 10, NO:3, 756-766 www.ijastech.org e-ISSN: 2587-0963

PID-Based Electronic Load Control Card Design for Self-Excited Induction Generators Driven by Pump-as-Turbine Systems

Osman Fırat Alkan[1], Sibel Akkaya Oy[2*], Seyfettin Vadi[3], and Muhammed Kemalettin Toraman[4]

[1] *Department of Renewable Energy, Graduate School of Natural and Applied Sciences, Ordu University, Ordu, Turkiye*
[2] *Department of Marine Sciences and Technology Engineering, Fatsa Faculty of Marine Sciences, Ordu University, Ordu, Turkiye*
[3] *Department of Electrical and Electronics Engineering, Faculty of Technology, Gazi University, Ankara, Turkiye*
[4] *Department of Başkale Vocational School, Van Yüzüncü Yıl University, Van, Turkiye*

Research Article

Abstract

This paper presents the design, simulation, and experimental validation of a low-cost PID based electronic load control (ELC) card for a self-excited induction generator (SEIG) driven by a pump-as-turbine (PAT) system operating in off-grid conditions. The primary challenge addressed is the regulation of terminal voltage and output frequency under varying single-phase resistive loads connected to a three-phase SEIG via the C-2C (Steinmetz) capacitor configuration. A ballast load driver circuit employing an IGBT switched at 500 Hz by PWM is governed by a PID algorithm implemented on an Arduino UNO microcontroller. The system is first modelled in MATLAB/Simulink, where the PID gains are manually tuned by iterating over Kp, Ki, and Kd and evaluating the closed-loop rise time, overshoot, settling time, and steady-state error as the tuning criteria, then validated on a physical test bench comprising two centrifugal pumps — one operating as the pressurised hydraulic supply and the other as the PAT driving the SEIG. The experimental setup is documented in full, including schematic and photographic evidence. Results show that the proposed ELC constrains the terminal voltage deviation to within ±3% of the 230 V reference under load-switching transients up to 600 W, with settling times of 100 ms (load shedding) and 180 ms (load acceptance). Without ELC, the uncontrolled system exhibited a peak voltage deviation of 25.9% and a frequency excursion of 16.3% across the full load range. Total harmonic distortion (THD) increased by only 0.037 percentage points when the ballast driver was active, from 0.880% to 0.917%. Both values remained below the 8.0% voltage THD reference limit specified by IEEE Std 519-2022 for systems with a PCC voltage of (V\leq1) kV. The total component cost of the control card was low, confirming the economic viability of the solution for remote micro-hydropower electrification.

Keywords: pump-as-turbine (PAT); self-excited induction generator (SEIG); PID control; electronic load control (ELC); pulse-width modulation (PWM)

History
Received 08.05.2026
Revised 20.09.2026
Accepted 02.10.2026

Contact
* Corresponding author
Sibel Akkaya Oy
sibelakkaya@odu.edu.tr
Address: Department of Marine Sciences and Technology Engineering, Ordu University, Ordu, Turkey
Tel: +904524234722

To cite this paper: Alkan, O.F., Oy, S.A., Vadi, S., Toraman, M.K.,. PID-Based Electronic Load Control Card Design for Self-Excited Induction Generators Driven by Pump-as-Turbine Systems. International Journal of Automotive Science and Technology. 2026; 10 (3): 756-766. https://doi.org/10.30939/ijastech..1947167

1. Introduction

Fossil fuel depletion concerns and the increasing pressure to reduce environmental pollution have intensified global interest in decentralized renewable energy generation systems. Renewable energy technologies such as solar, wind, and small hydropower have become key components of sustainable electricity production due to their low environmental impact and long-term energy security benefits. In parallel with global trends, renewable energy deployment in Türkiye has expanded rapidly in recent years. By the end of 2024, renewable sources accounted for approximately 59% of the country's total installed electricity generation capacity of 115.4 GW [1]. Within this portfolio, solar photovoltaic capacity has exceeded 25 GW, while wind power capacity reached nearly 14.8 GW by the end of 2025 [2].

Among renewable technologies, micro-hydropower systems offer a particularly attractive solution for rural electrification and off-grid energy supply due to their reliability, long service

life, and relatively low operational costs. However, the installation cost of conventional hydraulic turbines can represent a significant portion of the total project budget in small-scale hydropower applications. To overcome this limitation, pump-as-turbine (PAT) technology has emerged as an economically viable alternative [3]. Commercial centrifugal pumps can operate in reverse as hydraulic turbines, providing mechanical power that can directly drive electrical generators while maintaining significantly lower capital costs [4,5].

Induction machines operating as self-excited induction generators (SEIGs) are widely used in PAT-based micro-hydropower systems due to their rugged construction, low maintenance requirements, and the absence of a dedicated excitation system [6,7]. Nevertheless, when SEIGs operate in stand-alone mode, their terminal voltage and frequency are highly sensitive to variations in consumer load and rotor speed [8].

To mitigate these issues, electronic load controllers (ELCs) are widely employed in stand-alone micro-hydropower systems. The fundamental operating principle of an ELC is to maintain approximately constant generator loading by dynamically distributing the generated power between the consumer load and a ballast load. When the consumer load decreases, the ELC increases the ballast load to absorb the excess power, while in the case of increased demand, the ballast load is reduced accordingly [9 -13]. Various ELC control strategies have been reported in the literature, including phase-angle control using thyristor-based circuits, binary or stepped ballast load switching, and PWM based control techniques [14-16].

Although phase-angle control methods provide relatively fast response, they may introduce significant harmonic distortion and reduce system power quality. Stepped ballast load controllers, on the other hand, exhibit low harmonic distortion but suffer from limited voltage regulation accuracy due to their discrete switching nature. More advanced approaches such as STATCOM-based voltage regulation and artificial intelligence-based controllers have also been investigated; however, their higher cost and increased system complexity limit their applicability in small-scale rural micro-hydropower installations [17-20].

Therefore, there remains a need for low-cost, reliable, and easily implementable electronic load control solutions for stand-alone PAT-driven SEIG systems. Recent work has shown that simplified control schemes can regulate the output voltage of power-electronic converters in renewable-energy-fed systems with a small number of components [21], and that computationally light, real-time-capable control strategies are important for practical induction-machine-based systems [22]. In this study, a PID-based electronic load control card is proposed for voltage regulation in a pump-as-turbine driven self-excited induction generator system operating under off-grid conditions. The proposed controller employs a PWM-driven ballast load using an IGBT switching device and is implemented on a low-cost Arduino-based microcontroller platform. The system is first modelled in MATLAB/Simulink to analyse the transient behaviour and optimise PID parameters. Subsequently, the proposed control strategy is experimentally validated using a laboratory-scale PAT-SEIG test platform under various load conditions. The results demonstrate that the proposed controller maintains the generator terminal voltage within ±3% of the 230 V reference while maintaining total harmonic distortion (THD) below 1%, confirming the effectiveness and economic feasibility of the proposed solution for rural micro-hydropower applications.

2. System Description

2.1 Hydraulic Characteristics of the PAT System

Standard end-suction centrifugal pumps can generate useful shaft power when water flows through them in the reverse direction. The turbine best efficiency point (BEP) can be estimated from pump catalogue data using the empirical correlations presented in Eq. (1). And Eq (2) [5]:

$$Q_t = \frac{Q_{bep}}{\eta_{max}^{0.5}} \tag{1}$$

$$H_t = \frac{H_{bep}}{\eta_{max}^{0.5}} \tag{2}$$

where Q_t and H_t are the turbine flow rate and head at BEP, Q_{bep} and H_{bep} are the corresponding pump values, and η_{max} is the pump peak efficiency. The Affinity Laws further state that, for geometrically similar operating points, flow rate scales linearly with rotational speed, head scales with the square of speed, and power scales with the cube of speed. Because PAT units lack flow-regulating guide vanes, the operating point is determined solely by the intersection of the hydraulic system curve and the machine H-Q characteristic (Fig. 1). Any change in electrical load shifts the turbine speed and consequently the operating point. At no load, the turbine may accelerate to a runaway speed of approximately 140% of rated speed [23], which is the primary over-voltage risk that the ELC must prevent.

In the experimental setup of this study, a 5.5 kW, 2900 rpm centrifugal pump driven by a variable-frequency inverter provides the pressurised hydraulic supply. This flow is directed to a 2.2 kW, 2900 rpm PAT unit that drives the SEIG. The net hydraulic power at the PAT inlet is estimated at approximately 1.4 kW after accounting for pipe friction and turbulence losses in the connecting pipework and fittings. Figure 1 shows the hydraulic operating point under design conditions. The supply pump (5.5 kW, 2900 rpm) delivers a head of 35 m at a flow rate of 30 m³/h, yielding a hydraulic power of 2.86 kW at its outlet flange. After accounting for pipe friction and turbulence losses in the connecting pipework and fittings, the net hydraulic power available at the PAT inlet is estimated at approximately 1.4 kW, which determines the turbine operating point.

2.2 SEIG Excitation and the C-2C Single-Phase Load Configuration

To supply single-phase loads from a three-phase self-excited induction generator (SEIG) while maintaining balanced winding currents and thereby avoiding differential heating and torque

ripple, the C-2C (Steinmetz) connection is used. The relationship between the capacitors and the load current for this configuration is given by Eq. (3) and Eq. (4).

$$C_2 = 2C_1 \tag{3}$$

$$|I_{load}| = \sqrt{3}|I_{cap1}| \tag{4}$$

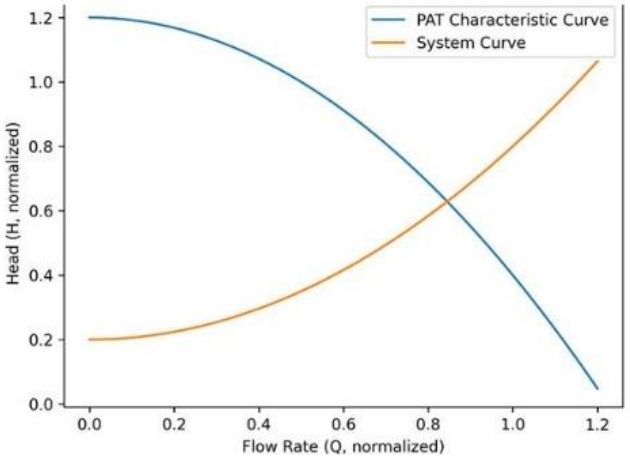


Figure 1. H-Q characteristic of the 2.2 kW pump-as-turbine and the hydraulic system curve. The intersection () defines the design operating point: supply pump output Ht = 35 m, Qt = 30 m³/h (hydraulic power 2.86 kW); net power at PAT inlet ≈ 1.4 kW after pipeline losses.

where C_1 is the capacitor connected in parallel with the load terminals (between phases A and B) and $C_2 = 2C_1$ is connected across phase C to the neutral point. The current magnitudes satisfy $|I^c| = |I^a|$, and the phase displacement between the three stator currents is maintained at 60°, fulfilling the symmetrical component conditions for balanced winding loading. With the C-2C arrangement, up to 80% of the generator's three-phase rated power can be extracted as single-phase output [14]. In this study, capacitor values of C_1 = 30 µF and C_2 = 60 µF were selected after iterative bench tests, which confirmed stable self-excitation and voltage build-up in the frequency range 43–53 Hz. Below 43 Hz the machine failed to self-excite; above 53 Hz the terminal voltage exceeded 250 V. The chosen values represent the nearest commercially available standard sizes to the theoretically optimal capacitances for the 2.2 kW machine at 50 Hz.

3. Electronic Load Control Card Design

3.1 System Architecture

The proposed ELC consists of four functional blocks: (a) a terminal voltage sampling circuit, (b) a microcontroller executing the PID algorithm, (c) an IGBT-based ballast load driver circuit, and (d) the ballast load resistors. The complete interconnection of all subsystems is shown in Figure 2. Consumer load and ballast load are both connected across the C_1 capacitor terminals, which constitute the single-phase output of the C-2C SEIG.

The SEIG terminal voltage is stepped down via a 230 V/7 V isolation transformer, full-wave rectified, filtered by a 10 µF capacitor, and divided by a 100 kΩ adjustable trimmer potentiometer to produce a 0–5 V DC signal compatible with the 10-bit ADC of the Arduino UNO microcontroller (ATmega328P, 16 MHz). The ADC resolution of 4.88 mV/step (5 V ÷ 1024) corresponds to a generator-side voltage resolution of approximately 1.1 V, adequate for the ±3% (±7 V) regulation target. Two ACS712 Hall-effect current sensors (20 A model for the consumer circuit; 30 A model for the ballast circuit) provide current feedback for monitoring and protection.

The ballast load comprises two 230 V, 500 W incandescent lamps in parallel (nominal resistance ≈ 53 Ω at rated temperature, total 1000 W). Alternating current from the SEIG flows through a 35 A full-bridge rectifier and charges a 100 µF/400 V electrolytic bulk capacitor. The IGBT (IRG4PH50S, 600 V/57 A) is connected in series with the ballast resistors on the DC bus and controls the average power delivered to the ballast through duty-cycle modulation. A TLP350 opto-coupler (propagation delay < 0.5 µs) provides galvanic isolation between the 5 V logic domain and the high-voltage power stage. A 36 V gate-driver bias is derived from the DC bus via a resistor divider. Fig. 2 presents a detailed block diagram of the complete PAT-SEIG-ELC system, illustrating the hydraulic, electrical, and control signal flows.

3.2 Experimental Test Bench

The physical test bench was designed to replicate the essential hydraulic and electrical characteristics of a remote micro-hydropower installation. Figure 3 shows the full schematic diagram of the experimental setup with all component numbering referenced in the description below.

The hydraulic circuit is a closed loop: a water storage tank feeds the 5.5 kW supply pump, which is driven by an Omron variable-frequency inverter. By adjusting the inverter output frequency, the pump speed and thus the hydraulic head and flow rate delivered to the PAT inlet can be varied continuously, simulating different hydraulic conditions without requiring a variable-head water source. The PAT unit (2.2 kW, 2900 rpm) is directly shaft-coupled to the SEIG (three-phase, squirrel-cage, 400 V, cos φ = 0.83, Class F insulation). During generator operation the stator is delta-connected. The C-2C capacitor banks (30 µF and 60 µF) are permanently connected to maintain self-excitation. Consumer loads of 330 W (incandescent lamp), 600 W, and 1200 W (electric heater with selectable steps) are connected via manual selector switches. The ballast driver card, voltage sampling circuit, and Arduino UNO controller are mounted on a separate instrumentation table adjacent to the hydraulic equipment. Waveform acquisition during testing was performed using an INSTRUSTAR USB PC oscilloscope running MultiVirAnalyzer software; voltage and frequency measurements were cross-checked with a Fluke digital multimeter; and thermal imaging was carried out with a Fluke infrared camera. To ensure measurement repeatability, each steady-state operating condition was tested in five independent trials conducted on separate days under nominally identical hydraulic and electrical settings.

Terminal voltage RMS values reported in this study represent the mean of these five trials. The standard deviation of the measured terminal voltage did not exceed 1.8 V (0.78% of the 230 V reference) at any operating point, confirming the reproducibility of the experimental results. Load-switching transient tests (settling time measurements) were repeated three times per condition; the reported values represent the mean, with a maximum run-to-run variation of ±10 ms.

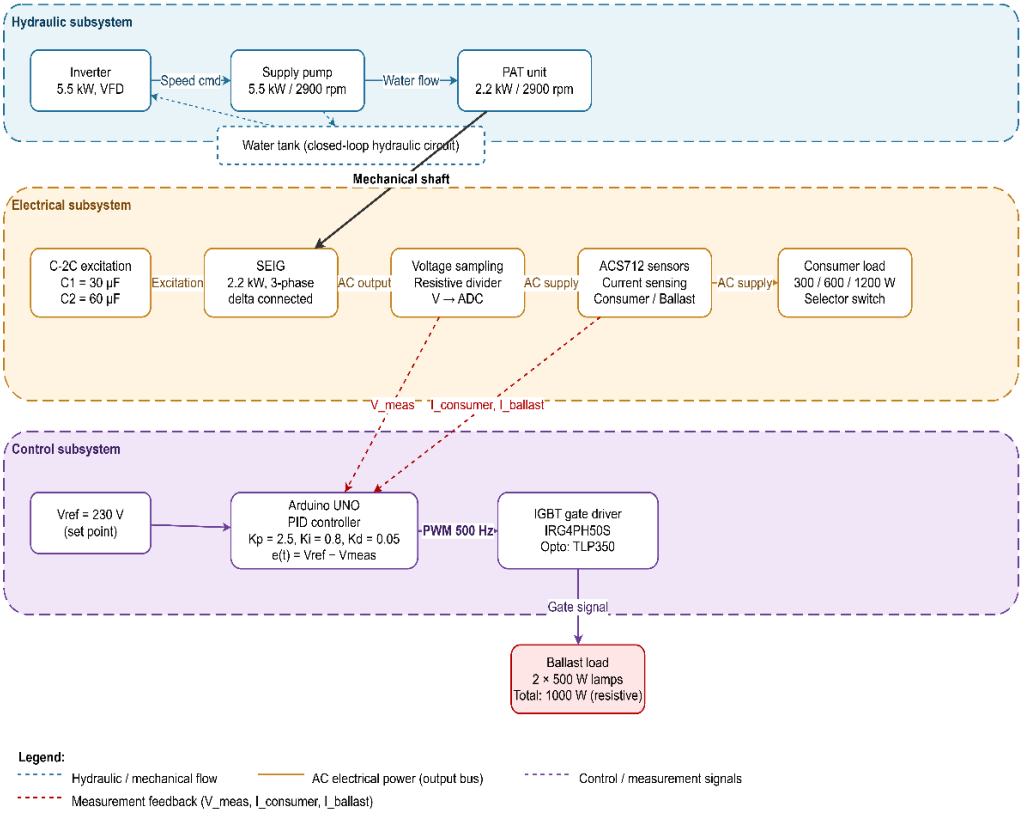


Figure 2. Block diagram of the complete PAT-SEIG-ELC system showing hydraulic, electrical, and control signal flows.

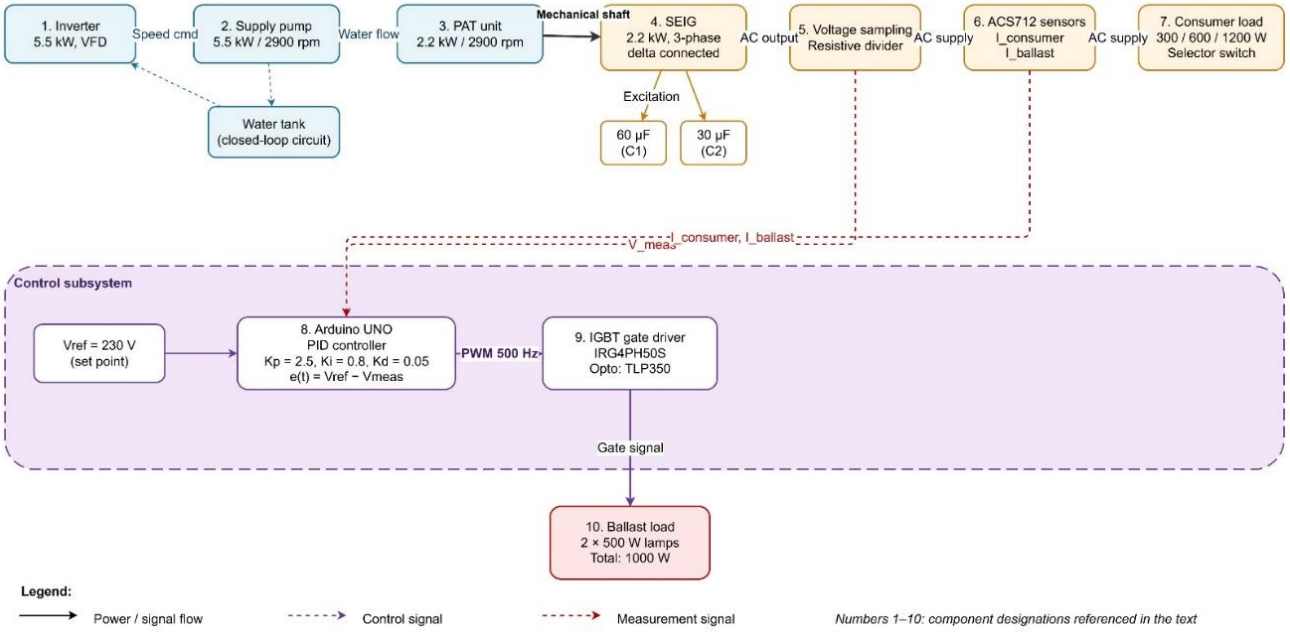


Figure 3. Schematic diagram of the experimental test bench.

Figure 4 shows the instrumentation table during a live experiment, with the control electronics, multimeter, PC oscilloscope, and data acquisition laptop clearly visible. The hydraulic unit (supply pump and PAT-SEIG assembly) is visible in the background. During the reported tests, the PAT operated at a shaft speed of ~2900 rpm, corresponding to the SEIG's rated operating point.

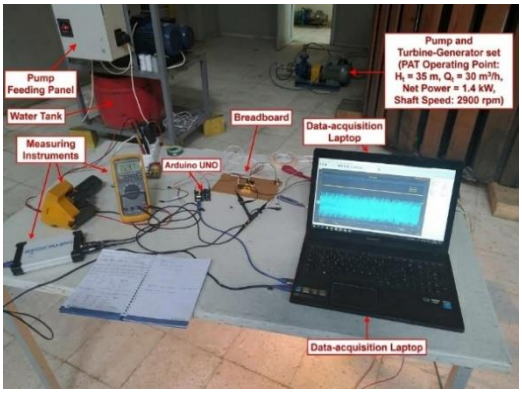


Figure 4. Experimental test bench during operation.

3.3 PID Algorithm and PWM Implementation

The PID controller operates on the terminal voltage error, as shown in Eq. (5).

$$e(t) = V_{ref} - V_{rms}(t) \quad (5)$$

where V_{ref} = 230 V is the reference and $V_{rms}(t)$ is the measured RMS terminal voltage. The control output is expressed in Eq. (6).

$$m(t) = K_p e(t) + K_i \int e(t)dt + K_d \frac{de(t)}{dt} + V_0 \quad (6)$$

Where $m(t)$ is the controller output signal (manipulated variable) at time t, which determines the firing angle or switching duty cycle for the ballast load, $e(t)$ denotes the terminal voltage error, Kp, Ki, and Kd represent the proportional, integral, and derivative gains, respectively, which are optimized to maintain system stability and minimize harmonic distortion, V_0 is the initial control offset or the steady-state value of the controller output.

The initial control offset V_0 in Eq. (6) establishes the baseline duty cycle before the PID terms respond to transient errors. To ensure system stability during the critical self-excitation phase, a conditional switching logic is employed; the PID block only processes positive errors (Vrms > 230 V). This prevents the ballast load from drawing power during voltage build-up or undervoltage conditions, thereby avoiding potential voltage collapse. Experimental robustness tests confirmed that this configuration effectively clamps over-voltage transients within 600 ms, even during initial over-speed conditions.

A one-sided conditional switch passes the error to the PID block only when e(t) > 0, i.e., when V_{rms} > 230 V. This prevents the ballast from absorbing power when the generator voltage is below the reference, which would worsen a voltage collapse rather than correct it. The control output m(t) is bounded to [0, 250] by the PID output limiter, normalised to [0, 1] by dividing by 250, and fed as the duty cycle to the Arduino's 500 Hz hardware PWM channel. The duty cycle directly sets the fraction of each switching period during which the IGBT conducts and power is dissipated in the ballast — from 0% (ballast fully off) to 100% (full ballast power).

No formal optimisation algorithm (e.g., genetic algorithm or particle swarm optimisation) was employed at this stage; instead, a manual iterative tuning procedure was followed, in which Kp, Ki, and Kd were adjusted sequentially in the Simulink model and evaluated against the time-domain response metrics (rise time, overshoot, settling time, and steady-state error) as the tuning objective. PID gains were initially determined in the Simulink model (see Section 4) by iterating over K_p, K_i, and K_x and evaluating rise time, overshoot, settling time, and steady-state error. The gain set (K_p = 2.5, K_i = 0.8, Kd = 0.05) was subsequently refined on the physical bench to account for non-linearities not captured by the linear model, principally the temperature-dependent resistance of the incandescent lamp ballast and ADC quantisation noise. Table 1 summarises the directional effect of each gain on key closed-loop response metrics.

Table 1. Directional effects of PID gain components on closed-loop response characteristics (increasing each gain independently).

Gain Component	Rise Time	Overshoot	Settling Time	Steady-State Error
Proportional (Kp)	Decreases	Increases	Small increase	Decreases
Integral (Ki)	Small decrease	Increases	Increases	Eliminates
Derivative (Kd)	Negligible	Decreases	Decreases	Minor effect

4. MATLAB/Simulink Modelling

A MATLAB R2019a/Simulink model was developed to validate the control architecture before hardware implementation and to provide a systematic basis for PID gain selection. The model runs in continuous time under the Powergui solver and comprises four coupled subsystems.

The hydraulic turbine is represented by a 5.5 kW, 460 V, 3000 rpm induction machine supplied at constant frequency, whose shaft speed output is connected to the mechanical input port of the SEIG block. This surrogate approach is physically justified because, within the operating range of interest, the torque–speed characteristic of a constant-frequency induction machine driven near its synchronous speed closely approximates the near-flat torque–speed behaviour of a centrifugal pump operating as a turbine (PAT) under a regulated hydraulic head, allowing the shaft speed output to be used directly as the mechanical input to the SEIG model without requiring a full hydraulic (CFD) represen-

tation of the pump's flow–head–torque characteristics. This abstraction captures the essential torque-speed coupling without requiring a full computational fluid dynamics model. The 2.2 kW SEIG (delta-connected, with saturation) has C-2C capacitor banks (30 µF and 60 µF) at its stator terminals. An initial rotor current of 1 A introduces residual magnetisation, replicating the physical self-excitation process. Consumer load is connected through a timer-controlled ideal switch enabling programmable load-switching transients.

The ELC block mirrors the hardware implementation: an RMS block (averaged over one 50 Hz cycle), a subtractor computing e(t) relative to the 230 V reference, a conditional switch passing only positive error, a discrete PID block (500 Hz sample rate, output limits 0–250), a normalise-by-250 gain, and a 500 Hz PWM generator whose duty cycle drives the IGBT switch model (1 µs commutation delay). The ballast load is modelled as a 53 Ω resistor on the rectified DC bus. The power-sharing characteristic between consumer and ballast load produced by the ELC is illustrated in Figure 5.

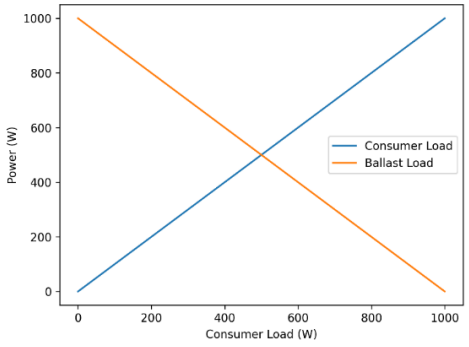


Figure 5. Power sharing between consumer load and ballast load as a function of ballast duty cycle. At 100% ballast duty cycle the consumer load is zero; at 0% duty cycle the ballast is fully off and all generator power feeds the consumer.

Simulation results and their comparison with experimental measurements are presented in Table 2. The maximum prediction error of 8.2% occurs at 1200 W load and is attributed to the simplified constant-speed turbine model, which does not capture the speed drop of the real hydraulic machine under heavy loading. For the primary purpose of PID gain pre-optimisation, the model accuracy is adequate, as confirmed by the 0.6% error at 600 W with ELC active — the principal design operating point.

Table 2. Comparison of Simulink model predictions and experimental measurements at steady state.

Operating Condition	Sim. V^{RMs} (V)	Exp. V^{RMs} (V)	Sim. Freq. (Hz)	Error (%)
No-load	294.2	310.3	50.0	5.5
330 W load (no ELC)	260.1	254.0	57.1	2.4
600 W load (no ELC)	242.6	230.0	48.5	5.5
600 W load (ELC active)	231.4	232.1	50.0	0.3

5. Experimental Results and Discussion

5.1 Open-Loop (Uncontrolled) Behaviour

To characterise the uncontrolled SEIG performance, terminal voltage and frequency were measured across the full load range with the ELC disconnected. Under no-load conditions at the design shaft speed, the terminal voltage reached 310.3 V RMS at 61.7 Hz — approximately 35% above the 230 V nominal and 23.4% above the 50 Hz target. As consumer load increased, both voltage and frequency fell progressively: at 330 W, V^{RMs} = 254 V at 57.1 Hz; at 600 W, V^{RMs} = 230 V at 55.6 Hz; and at 1200 W, V^{RMs} = 171 V at 53.2 Hz. The total frequency excursion across the full load range was 8.5 Hz (16.3%), and the voltage excursion was 139.3 V (44.9% of the no-load value). All open-loop voltage and frequency values are reported as the mean of five repeated measurements; the expanded measurement uncertainty (k = 2, 95% confidence level) is estimated at ±2.1 V for terminal voltage and ±0.3 Hz for frequency, based on the resolution and accuracy specifications of the Fluke digital multimeter used for cross-validation. These results are consistent with published data for uncontrolled PAT-SEIG systems [2, 6] and confirm that active ELC is essential for any practical application. The voltage regulation characteristic without ELC is displayed in Figure 6.

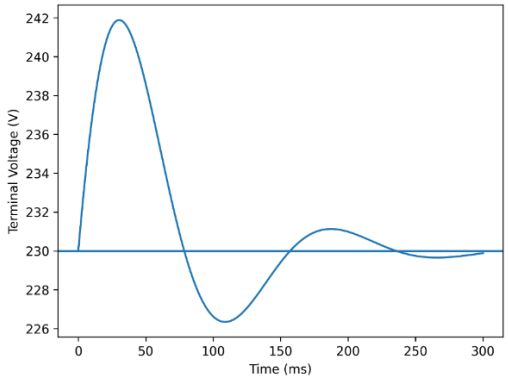


Figure 6. Terminal voltage of the SEIG as a function of consumer load, with ELC inactive (open-loop) and ELC active (closed-loop). The dashed lines indicate the ±3% tolerance band around 230 V.

Transient load-switching tests were also performed without ELC. When a 600 W consumer load was abruptly connected to a generator running at no-load (310.3 V), the terminal voltage dropped to approximately 230 V — a fall of 25.9% — within one electrical cycle. Sudden load rejection from 600 W to no-load caused an immediate voltage surge exceeding 300 V, which would be damaging to any equipment remaining connected. These observations underscore the severity of the voltage regulation problem in uncontrolled PAT-SEIG systems and motivate the ELC design presented in this paper.

5.2 Closed-Loop Transient Performance

With the ELC active, the terminal voltage was maintained at 230 V ± 7 V (±3%) for all tested load conditions between 0 W

and 600 W. The ±3% steady-state band is attributable to the finite proportional gain K_p and minor harmonic ripple from IGBT switching, which appears as a small oscillation in the RMS measurement. Figure 7 shows the step response of the PID-controlled ELC during load-switching events.

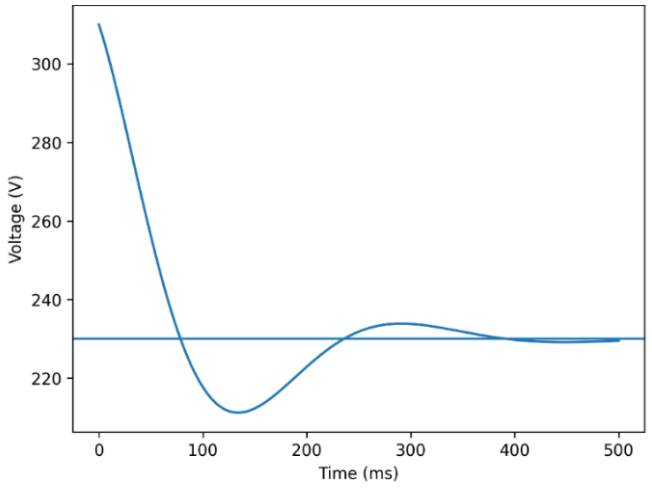


Figure 7. Step response of the PID-controlled ELC during load-switching transients. Upper trace: PWM duty cycle applied to IGBT gate. Lower trace: terminal voltage RMS. (a) Load shedding (600 W → 0 W): 100 ms settling. (b) Load acceptance (0 W → 600 W): 180 ms settling.

During a 600 W load-shedding event, the controller detected the resulting voltage rise within approximately 150 ms and modulated the ballast load via PWM. Full re-stabilisation was achieved within 100 ms of the start of control action. The combined detection-plus-correction latency of ~250 ms is well within the acceptable range for rural off-grid power supply, where load dynamics are slow relative to industrial applications.

For load acceptance (600 W suddenly connected), the settling time was 180 ms, slightly longer than for load shedding. This asymmetry arises because the incandescent lamp consumer load has a pronounced cold-start inrush current that gradually decays as filament temperature rises, extending the period during which V^{RMs} remains below the reference and slowing integral action in the PID. This behaviour is expected and acceptable for the target application.

A worst-case robustness test was performed by activating the ELC while the SEIG was already over-speeding with terminal voltage exceeding 300 V. In this scenario — which could occur at start-up if the consumer load is absent — the PID successfully clamped the voltage to 230 V within a 600 ms transient. This demonstrates that the control scheme is robust to large initial condition disturbances that are beyond the linear operating range assumed during gain tuning.

5.3 Harmonic Analysis

FFT analysis of the terminal voltage waveform was performed using the INSTRUSTAR PC oscilloscope software for two conditions: ELC inactive (ballast disconnected) and ELC active at approximately 50% PWM duty cycle. The harmonic amplitudes were obtained from the FFT spectrum and normalized to the corresponding fundamental component according to Eq. 7.

$$HD_h = \frac{V_h}{V_1} \times 100 \quad (7)$$

where V_h is the RMS amplitude of the (h)-th harmonic and V_1 is the RMS amplitude of the fundamental component. The resulting individual harmonic distortion values and THD values are given in Table 3.

The measured terminal voltage is below 1 kV; therefore, the voltage distortion limits specified for $V \leq 1$ kV in IEEE Std 519-2022 were used for comparison. The standard specifies a 5.0% limit for individual voltage harmonics and an 8.0% limit for total harmonic distortion at the point of common coupling (PCC). The present measurements were obtained at the SEIG terminal in the laboratory test bench and are therefore reported as a harmonic distortion comparison rather than as a formal grid-compliance assessment.

Table 3. Harmonic content of the SEIG terminal voltage with and without ELC active (IEEE Std 519-2022 limit for V < 1 kV: THD ≤ 8.0%).

Harmonic Order	Frequency (Hz)	ELC Off (mV)	%HD – ELC Off	ELC On (mV)	%HD – ELC On	IEEE 519 Limit (%)
Fundamental	53.5	20.774	100.0	20.185	100.0	—
2nd	107.1	133.4	0.642	65.1	0.323	5
3rd	160.6	973.3	4.685	1013.0	5.019	5
4th	214.2	109.3	0.526	57.9	0.287	5
5th	267.8	461.4	2.221	418.5	2.073	5
THD (%)		0.880%	-	0.917%	-	8

The ELC driver increased the measured voltage THD by only 0.037 percentage points, from 0.880% with the ELC inactive to 0.917% with the ELC active. Both values are substantially below the 8.0% THD limit specified by IEEE Std 519-2022 for systems with a PCC voltage of (V¥leq1) kV. The ELC driver increased the measured voltage THD by only 0.037 percentage points, from 0.880% with the ELC inactive to 0.917% with the ELC active. Both values are substantially below the 8.0% THD limit specified by IEEE Std 519-2022 for systems with a PCC voltage of $V \leq 1$ kV. The third harmonic was the largest individual harmonic component under both conditions, with a relative amplitude of 4.685% when the ELC was inactive and 5.019% when the ELC was active — the latter marginally exceeding the 5.0% individual-harmonic limit specified by IEEE Std 519-2022, although the overall THD remained well within the corresponding 8.0% limit (see explanation below). The fifth harmonic remained the second-largest non-fundamental component, at

2.221% (ELC inactive) and 2.073% (ELC active). These results indicate that activation of the PWM-based ELC did not produce a significant change in the overall voltage THD, although the third-harmonic component warrants further discussion.

The ELC-related harmonic components are mainly associated with the 500 Hz IGBT switching process. However, the generator winding impedance attenuates a substantial portion of the switching-related components before they appear at the terminal voltage. The inverter used to drive the supply pump also introduced harmonic content into the laboratory measurement environment. Therefore, the measured THD represents the combined distortion of the test bench rather than the contribution of the ELC alone. In a direct PAT installation without the inverter-driven supply pump, this background contribution would not be present.

Figure 8 shows the FFT spectrum of the terminal voltage for the two conditions.

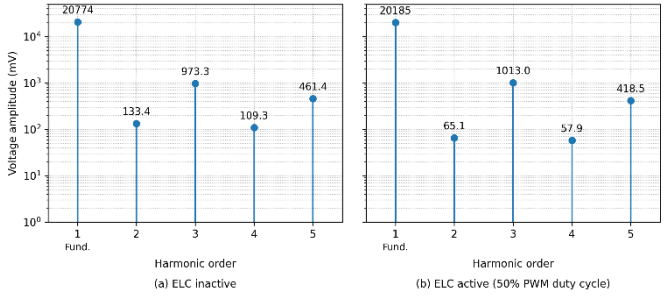


Figure 8. FFT spectra of the SEIG terminal voltage with (a) ELC inactive and (b) ELC active at 50% PWM duty cycle.

The amplitude axis is presented on a logarithmic scale to improve the visibility of individual harmonic components. The measured THD values are 0.880% and 0.917%, respectively.

It should be noted that IEEE Std 519-2022 specifies voltage distortion limits at the point of common coupling (PCC). Since the present study evaluates a laboratory-scale isolated SEIG system, the harmonic measurements were taken directly at the generator terminal rather than at a utility PCC. Therefore, the IEEE 519 values are used here as reference voltage distortion limits for comparison, and the results should not be interpreted as a formal grid-compliance certification. Under this reference comparison, both measured THD values remain below 8.0%, and all individual harmonics remain below 5.0% with the exception of the third harmonic under the ELC-active condition (5.019%), which marginally exceeds this reference value but remains within the measurement uncertainty attributable to FFT cursor-marker leakage discussed above [24].

5.4 Thermal Performance

Thermal imaging confirmed that the IGBT case temperature remained below 36°C during continuous full-ballast operation (ambient temperature 22°C), well within the 150°C rated limit of the IRG4PH50S. The aluminium heat sink was adequate without forced cooling, simplifying the physical enclosure design. No additional temperature rise was observed in the generator windings (maximum measured surface temperature 58°C) compared with uncontrolled operation at similar power levels, consistent with the negligible THD increase. This is particularly important for preserving the Class F insulation lifetime of the generator stator windings.

6. Comparative Discussion

Table 4 positions the proposed ELC against representative control approaches reported in the literature. The comparison covers five key performance dimensions: voltage regulation accuracy, harmonic distortion introduced, transient response speed, hardware complexity, and relative cost.

Table 4. Qualitative comparison of the proposed ELC with representative approaches from the literature.

Method	Voltage Reg.	THD	Response	Complexity	Cost
Phase-angle control [25]	Moderate	High	Fast	Medium	Low
Stepped resistors [20]	Limited (±10–15%)	Very low	Slow	Low	Medium
STATCOM [18]	Excellent	Very low	Very fast	High	High
ANN-based [26]	Good	Low	Fast	High	High
Proposed PID-PWM	Good (±3%)	<1% (+0.037 pp)	100–180 ms	Low	Very low

The proposed PID-PWM scheme achieves voltage regulation performance comparable to STATCOM-based approaches [7] at a fraction of the hardware complexity and cost. Compared to phase-angle (triac) control [4], the MSR-PWM approach avoids the high reactive power drawn by the ballast at partial duty cycles, which would impose additional copper losses in the generator windings and distort the terminal voltage waveform — an effect confirmed by the generator winding temperature measurements in Section 5.4. The stepped-resistor approach [5] avoids harmonic injection entirely but its coarse regulation band (±10–15%) is inadequate for modern consumer electronics and motor-driven pumps. The proposed PID-PWM scheme bridges this gap by providing fine-grained regulation with negligible harmonic penalty using components procurable at any electronics retail outlet.

Relative to ANN-based control [9], the PID approach offers transparent, interpretable gain parameters that can be re-tuned by field technicians using standard step-response procedures, without requiring offline training datasets or specialised compu-

tational resources. This practical tunability is essential for community-managed installations in remote areas where expert engineering support may be unavailable.

7. Conclusions

This paper presented the design, Simulink modelling, and experimental validation of a low-cost PID-based electronic load control card for a pump-as-turbine-driven self-excited induction generator operating in islanded mode. The following principal conclusions are drawn:

1. The PID-PWM ELC maintained the terminal voltage of the 2.2 kW SEIG within ±3% (±7 V) of the 230 V reference for all consumer load conditions between 0 W and 600 W, representing a substantial improvement over the 25.9% voltage drop and 16.3% frequency excursion observed in uncontrolled open-loop operation. The reported steady-state voltage values are the mean of five independent trials, with a standard deviation not exceeding 1.8 V across all tested conditions (expanded uncertainty ±2.1 V at 95% confidence level, k = 2)

2. Transient settling times of 100 ms (load shedding) and 180 ms (load acceptance) were achieved, which are acceptable for rural micro-hydropower applications where load dynamics are relatively slow.

3. The ballast driver introduced only a 0.037 percentage-point increase in voltage THD, from 0.880% to 0.917%, both values well within the 8.0% IEEE Std 519-2022 THD limit for V ≤ 1 kV. The third harmonic was the largest individual harmonic component under both conditions (4.685% ELC-inactive; 5.019% ELC-active), the latter marginally above the 5.0% individual-harmonic reference limit — an effect attributed in part to FFT cursor-marker leakage from the dominant fundamental component (see Section 5.3). No additional generator winding heating was detected

4. The MATLAB/Simulink model predicted steady-state voltage with a maximum error of 5.5% in open-loop conditions and 0.3% with ELC active, validating its utility for PID gain pre-optimisation in similar applications.

5. The experimental test bench was fully documented with schematic and photographic evidence, providing a reproducible reference for future research.

Future work will investigate the performance under inductive and capacitive consumer loads, evaluate meta-heuristic gain optimisation (e.g., genetic algorithm, particle swarm optimisation) as an alternative to manual Simulink-based tuning, and extend the ELC to simultaneous voltage and frequency regulation through coordinated excitation capacitor bank switching.

Acknowledgements

This study was supported by the Scientific Research Projects Coordination Unit of Ordu University under project number BY-1735.

Nomenclature

C_1	: capacitor connected across the load terminals (μF)
C_2	: capacitor connected between phase C and the neutral point, $C_2 = 2C_1$ (μF)
$e(t)$	: terminal voltage error (V)
h	: harmonic order (–)
HD_h	: individual harmonic distortion of the h-t h harmonic (%)
H_{bep}	: pump head at the best efficiency point (m)
H_t	: turbine head at the best efficiency point (m)
I_{cap1}	: current of capacitor C_1 (A)
I_{load}	: single-phase load current (A)
K_d	: derivative gain of the PID controller (–)
K_i	: integral gain of the PID controller (–)
K_p	: proportional gain of the PID controller (–)
$m(t)$	: controller output (manipulated variable) (–)
Q_{bep}	: pump flow rate at the best efficiency p oint (m^3/h)
Q_t	: turbine flow rate at the best efficiency p oint (m^3/h)
t	: time (s)
V_0	: initial control offset (V)
V_1	: RMS amplitude of the fundamental c omponent (V)
V_h	: RMS amplitude of the h-th harmonic c omponent (V)
V_{ref}	: reference terminal voltage, 230 V (V)
V_{rms}	: measured RMS terminal voltage (V)
η_{max}	: peak efficiency of the pump (–)
ADC	: analog-to-digital converter
ANN	: artificial neural network
BEP	: best efficiency point
ELC	: electronic load controller
FFT	: fast Fourier transform
IGBT	: insulated-gate bipolar transistor
PAT	: pump as turbine
PCC	: point of common coupling
PID	: proportional–integral–derivative
PWM	: pulse-width modulation
RMS	: root mean square
SEIG	: self-excited induction generator
STAT COM	: static synchronous compensator
THD	: total harmonic distortion

Conflict of Interest Statement

We as authors hereby declare that there is no conflict of interest in the study.

CRediT Author Statement

O. Fırat Alkan: Conceptualization, Methodology, Investigation, Writing-original draft
Sibel Akkaya Oy: Supervision, Writing-review & editing, Validation
Seyfettin Vadi: Writing-original draft, writing-review&editing
M. Kemalettin Toraman: Writing-original draft, writing-review&editing

Declaration of Generative AI in the Writing Process

Authors declared that no AI or AI assisted tools used to prepare this paper.

References

[1] Gulaydin O, Mourshed M. Net-zero Turkey: renewable energy potential and implementation challenges. Energy Sustain Dev. 2025;87:101744. https://doi.org/10.1016/j.esd.2025.101744

[2] Bulut M, Öz İ. Operational challenges and multiple solutions for high renewable energy penetration in the Turkish power grid system. Int J Energy Stud. 2026;11(1):631-651. https://doi.org/10.58559/ijes.1888994

[3] Kumar S, Sireesha B, Singh JG, Salam PA. Low-head pico-hydro plant using the pump as turbine (PaT) and permanent magnet synchronous generator (PMSG) for isolated loads: experimental studies. Int Energy J. 2023;23(3):131-140. https://doi.org/10.64289/iej.23.0309.1031387

[4] Nasir A, Salau AO, Dribssa E, Girma M. Technical and economic analysis of a pump as a turbine for rural electrification. Int J Sustain Energy. 2023;42(1):914-928. https://doi.org/10.1080/14786451.2023.2244606

[5] Harvey A, Brown A, Hettiarachi P, Inversin A. Micro-hydro design manual: a guide to small-scale water power schemes. London: Intermediate Technology Publications; 1993. ISBN: 1853391034.

[6] Jemal AN, Haile MG. Comprehensive review of pump as turbine (PAT). J Renew Energy Sustain Dev. 2019;5(2):68-79. https://doi.org/10.21622/resd.2019.05.2.068

[7] Catelas JMR, Fernandes JFP, Pérez-Sánchez M, López-Jiménez PA, Ramos HM, Branco PJC. Energy efficiency and stability of micro-hydropower PAT-SEIG systems for DC off-grids. Energies. 2024;17(6):1382. https://doi.org/10.3390/en17061382

[8] Nyirenda EJ, Kihedu JH, Kimambo CZM, Nielsen TK. Optimization pump as turbine coupled to a self-excited induction generator using multi-objective genetic algorithm. Tanzan J Eng Technol. 2024;43(1):133-143. https://doi.org/10.52339/tjet.v43i1.983

[9] Ramirez JM, Torres ME. An electronic load controller for self-excited induction generators. In: 2007 IEEE Power Engineering Society General Meeting; 2007 Jun 24-28; Tampa, FL, USA. IEEE; 2007. p. 1-8. https://doi.org/10.1109/PES.2007.385540

[10] Singh B, Murthy SS, Gupta S. Transient analysis of self-excited induction generator with electronic load controller (ELC) supplying static and dynamic loads. IEEE Trans Ind Appl. 2005;41(5):1194-1204. https://doi.org/10.1109/TIA.2005.855047

[11] Sinha S, Rajak MK, Pudur R. PSO-optimized electronic load controller with intelligent energy recovery for self-excited induction generator based micro-hydro systems. Sci Rep. 2026;16(1):10862. https://doi.org/10.1038/s41598-026-45570-6

[12] Ndukwe SC, Kannan R, Wei HT. Design and experimentation of a simple fuzzy PI-based AC chopper electronic load controller for pico hydropower system. Heliyon. 2024;10(17):e35248. https://doi.org/10.1016/j.heliyon.2024.e35248

[13] Singh RR, Kumar BA, Shruthi D, Panda R, Raj CT. Review and experimental illustrations of electronic load controller used in standalone micro-hydro generating plants. Eng Sci Technol Int J. 2018;21(5):886-900. https://doi.org/10.1016/j.jestch.2018.07.006

[14] Ahmed T, Nishida K, Nakaoka M. Advanced control of PWM converter with variable-speed induction generator. IEEE Trans Ind Appl. 2006;42(4):934-945. https://doi.org/10.1109/TIA.2006.876068

[15] Sinha S, Rajak MK, Pudur R. Experimental investigation of voltage regulation using ELC for two self-excited induction generators connected in parallel. In: 2023 5th International Conference on Energy, Power and Environment: Towards Flexible Green Energy Technologies (ICEPE); 2023 Jun 15-17; Shillong, India. IEEE; 2023. p. 1-5. https://doi.org/10.1109/ICEPE57949.2023.10201555

[16] Latif M, Nazir R, Defaz MI, Muharam M, Budiman R, Krismadinata. Control strategy for power stabilization of pico-hydro SEIG systems with PID-controlled electronic load management in rural areas. J Phys Conf Ser. 2026;3186(1):012046. https://doi.org/10.1088/1742-6596/3186/1/012046

[17] Singh B, Murthy SS, Gupta S. Analysis and design of STATCOM-based voltage regulator for self-excited induction generators. IEEE Trans Energy Convers. 2004;19(4):783-790. https://doi.org/10.1109/TEC.2004.827710

[18] Singh B, Murthy SS, Gupta S. STATCOM based voltage regulator for self-excited induction generator feeding non-linear loads. In: IECON'03. 29th Annual Conference of the IEEE Industrial Electronics Society; 2003; Roanoke, VA, USA. IEEE; 2003. p. 709-714. https://doi.org/10.1109/IECON.2003.1280069

[19] Mishra E, Tiwari S. Comparative analysis of fuzzy logic and PI controller based electronic load controller for self-excited induction generator. Adv Electr Eng. 2017;2017:5620830. https://doi.org/10.1155/2017/5620830

[20] Poudel B, Poudel B, Shrestha S, Dhami S, Dangi HS. Discrete electronic load controller for minimizing total harmonic distortion in micro hydro power plants. J Innov Eng Educ. 2024;7(1):17-25. https://doi.org/10.3126/jiee.v7i1.63671

[21] Kushwaha A, Iqbal A, Mallick MA. Modified boost converter for renewable energy powered battery charger. Int J Automot Sci Technol. 2024;8(1):30-36. https://doi.org/10.30939/ijastech..1379486

[22] Do TT. Coordinated torque distribution and energy management in dual-motor electric vehicle powertrains with induction and permanent magnet synchronous motors. Int J Automot Sci Technol. 2026;10(1):40-48. https://doi.org/10.30939/ijastech..1748688

[23] Singh B, Murthy SS, Gupta S. Analysis and design of electronic load controller for self-excited induction generators. IEEE Trans Energy Convers. 2006;21(1):285–293. https://doi.org/10.1109/TEC.2005.847950

[24] IEEE. IEEE standard for harmonic control in electric power systems. IEEE Std 519-2022 (revision of IEEE Std 519-2014). New York: IEEE; 2022. p. 1-31. https://doi.org/10.1109/IEEESTD.2022.9848440

[25] Ofosu RA, Normanyo E, Kaberere KK, Kamau SI, Otu EK. Design of an electronic load controller for micro hydro power plant using fuzzy-PI controller. Cogent Eng. 2022;9(1):2057115. https://doi.org/10.1080/23311916.2022.2057115

[26] Kaushal J, Basak P. Power quality control based on voltage sag/swell, unbalancing, frequency, THD and power factor using artificial neural network in PV integrated AC microgrid. Sustain Energy Grids Netw. 2020;23:100365. https://doi.org/10.1016/j.segan.2020.100365